Energy Storage and Conversion 2024, 2(3), 515.
https://doi.org/10.59400/esc.v2i3.515

Article

Heat transfer characteristics in Williamson fluid flow in a vertical channel with chemical reaction and entropy production

Amala Olkha, Mukesh Kumar*

Department of Mathematics, University of Rajasthan, Jaipur 302004, India
*** Corresponding author:** Mukesh Kumar, mukeshkumar2011992@gmail.com

CITATION

Olkha A, Kumar M. Heat transfer characteristics in Williamson fluid flow in a vertical channel with chemical reaction and entropy production. Energy Storage and Conversion. 2024; 2(3): 515. https://doi.org/10.59400/esc.v2i3.515

ARTICLE INFO

Received: 26 March 2024
Accepted: 21 June 2024
Available online: 1 July 2024

Abstract: This research endeavor investigates the natural convection flow of Williamson fluid in the region between two vertical parallel flat plates via a porous medium. Impacts of viscous dissipation, joule heating, exponential space, and thermal-dependent heat sources (ESHS/THS) are invoked. Mass transfer is also studied in accounting for chemical reaction impact. The governing non-linear PDEs are reduced to ODEs in non-dimensional form under adequate transformation relations. The numerical technique, namely, Runge-Kutta fourth-order, is utilized to tackle the problem with the shooting method. Additionally, second-law analysis is presented in terms of entropy production. The effects of numerous regulating parameters occurred in the problem relevant to flow, heat and mass transport, and entropy production are discussed via graphical mode of representation. Moreover, the quantities of physical significance are computed, displayed in graphical form, and discussed. For verification of acquired results, a comparison is also made using HPM with prior research, which was found to be in excellent agreement. It is concluded that the fluid temperature field enhances with upsurging values of pertinent parameters. The influence of the convective surface parameter and order of reaction are found to make augmentation in mass diffusion. Further, the effect of joule heating is noticed to increase the rate of heat transfer, while the reverse scenario is observed with upsurging values of heat source parameters. The influence of viscous dissipation is seen to increase entropy production.

Keywords: Williamson fluid; velocity slip; THS; ESHS; viscous dissipation; porous medium; joule heating; chemical reaction; entropy production; convective boundaries; HPM

1. Introduction

The channel flows are the fundamental configurations in fluid dynamics. The study of convection flow in channels has been a prominent field of research interest for its important engineering applications, e.g., in electrochemical processes, heat exchangers, solar energy collectors, fibrous insulation, and so forth. Several researchers have considered the natural convection problems of viscous fluids in the region between two vertical flat plates, including Bruce and Na [1], Aung et al. [2], Vajravelu and Sastri [3], Rajagopal and Na [4], Cheng et al. [5], Ziabakhsh and Domairry [6], Narahari and Dutta [7], Kargar and Akbarzade [8], Rashidi et al. [9], Hatami et al. [10], etc.

The overhead investigations were carried out for the clear fluid flows. None of these studies considered flow via a porous medium. In thermal-free convection via porous medium, the fluid flow is driven by buoyancy forces. These forces occur because of density variations due to temperature gradients in the fluid. The interest in the study of convection via porous medium is inspired by its significance in widespread practical and engineering applications, for example, solar power

collectors, drying processes, heat removal in nuclear reactors, groundwater pollution, thermal insulation, etc. A considerable number of studies on convection flow problems of viscous fluids via porous medium in the region between two vertical parallel plates under the influence of Lorentz force have been reported by many researchers, such as Rapits et al. [11], Chamkha [12], Singh and Pathak [13], Das et al. [14], and many others. MHD flow continues to be of interest to researchers due to its wide range of practical applications in manufacturing processes, MHD power generators, astrophysical fluid dynamics, plasma aerodynamics, and geophysical fluid dynamics. Besides, in medical therapies like laparoscopic treatment, MHD with joule heating plays a significant role. In recent years, Asha and Sunitha [15], Swain et al. [16], Ramesh et al. [17], Ali et al. [18], etc. have examined the effects of MHD with joule heating.

Williamson fluid, a pseudoplastic non-Newtonian fluid, was introduced by Williamson [19]. The investigations of such fluid flows are significant because of their important practical applications, such as in the drawing of polymer sheets, the production of adhesives, photographic film production, and so on. Vasudev [20] investigated heat transport in the peristaltic flow of Williamson fluid in the region between horizontal parallel plates via a porous medium. Considering the impact of Lorentz force, the natural convection flow of Williamson fluid in the region between vertical parallel plates via porous medium was proposed by Subramanyam et al. [21]. Swaroopa and Prasad [22] proposed free convection Williamson flow in the region between parallel walls under consideration of radiation and Lorentz force impact. An analytical investigation of Williamson fluid-free convective flow in an upright channel with permeable walls, considering viscosity and radiation effects, was presented by Ajibade et al. [23]. Forced convection in Williamson flow via a porous medium was carried out by Qawasmeh et al. [24]. Pattanaik et al. [25] have analysed Williamson flow via porous medium in the existence of nanoparticles in a parallel plate channel due to thermal buoyancy, considering Lorentz force and radiation impacts. Usman et al. [26] have examined heat transport in Williamson fluid flow in a ciliated channel with permeable walls under the influence of Lorentz force via porous media.

In nature and industries, many transport processes occur where thermal and mass transport take place parallelly as a consequence of the joint buoyancy effects of thermal and species diffusion. The heat and mass transport phenomenon is also encountered in chemical process industries, for instance, polymer production and food processing. The occurrence of reactions and their order in such phenomena influence the performance and features of the product obtained. Grosan et al. [27] examined the impact of thermophoretic transport of particles in mixed convective heat and mass transport in a vertical parallel plate channel. Reaction influence on convection flow of power law fluid in the existence of porous medium, invoking heat and mass transport, was examined by Ibrahim et al. [28]. Uwanta and Hamza [29] discussed the impact of suction or injection on the exothermic reaction of Arrhenius kinetics, thermal diffusion, and the time-dependent convective flow of viscous Newtonian fluid in the region between two infinite upright parallel permeable plates. Prasannakumara et al. [30] studied reaction and radiation influence on Williamson fluid flow with nanoparticles in porous medium influenced by stretchy surfaces. Singh and Kumar [31] investigated heat and mass transmission in micropolar fluid flow in porous

channels, considering chemical reactions with radiation influence. Mallikarjun et al. [32] analysed fully developed mixed convection flow in a vertical channel, considering heat production, absorption, and reactions of first order. Thermal and mass transport in the convective flow of Williamson fluid outside a cylinder via porous medium, under assumptions of the boundary layer, was investigated by Loganathan and Dhivya [33]. Huang [34] has examined thermal and mass transport in convective flow via porous medium along an inclined surface, considering Lorentz force influence. Nazir et al. [35] have considered surface chemical reactions in the flow of Walter's B fluid past a paraboloid, including heat and mass diffusion. Olkha and Kumar [36] have reported heat and mass transport in free convection flow of non-Newtonian fluid via porous medium in the region between two vertical cylinders, considering chemical reaction impact. Olkha and Kumar [37] have also investigated melting heat transport in non-Newtonian fluid flow via porous medium produced by a curved surface stretching non-linearly, including mass transport and reaction influence.

The consideration of convective boundary conditions in heat transport problems is significant in engineering processes, e.g., thermal energy storage, gas turbines, nuclear plants, and so forth. Srinivas et al. [38] studied thermal and mass diffusion in the pulsating flow of viscous Newtonian fluid in a horizontal channel via porous medium, considering slip flow and convective boundary constraints, including Lorentz force and chemical reaction. Oyelakin et al. [39] employed convective surface boundary conditions, including velocity slip in time-dependent non-Newtonian flow in the existence of nanoparticles including influence of heat transport characteristics. Such constraints on the convection slip flow of Williamson fluid produced by a stretchy surface, considering Lorentz force and Joule heating, were employed by Sharada and Shankar [40]. Zeeshan et al. [41] explored the radiative Couette-Poiseuille flow of nanofluid in a channel with chemical reactions considering convective boundaries, Joule heating, activation energy, and viscous dissipation. Convective boundary conditions to discuss heat transport in the flow of Casson fluid in the region between inclined permeable parallel plates, invoking the impacts of flow-thermal properties, were considered by Neeraja et al. [42]. Jagadeesh and Reddy [43] have employed convective boundary conditions in 3-D convection non-Newtonian couple stress flow in the existence of nanoparticles influenced by a stretchable sheet, considering Lorentz force, radiation, and reaction.

The exponential space-dependent heat source procedure is probably more suited for excellent thermal processes since a minor size augmentation of the heat source leads to a significant improvement in the thermal field. Several researchers have considered exponential space- and thermal-dependent heat sources (ESHS/THS) in their studies conducted on viscous Newtonian and non-Newtonian fluid flows in various aspects, including Zaigham Zia et al. [44], Thriveni et al. [45], Mahanthesh et al. [46], Nagaraja and Gireesha [47], Swain et al. [48], Hasibi et al. [49], Sharma et al. [50], etc.

Entropy, a key thermodynamic irreversibility parameter, occurs in the second law of thermodynamics. The analysis of entropy production makes a significant contribution to thermal systems design decisions and thus supports optimization of cost and energy in science and engineering areas like the cooling of electronic devices,

heat exchangers, energy storage systems (Yessef et al. [51], Chojaa et al. [52], Loulijat et al. [53], and Hamid et al. [54]), etc. Bejan [55,56] presented pioneering work on entropy production and its optimization. Baytas [57] analysed entropy production in free convection via porous medium along with thermal transport and mass transport in a tilted permeable enclosure. Makinde and Eegunjobi [58] proposed the rate of entropy and Bejan number in viscous couple stress flow in an upright channel filled with porous material in the existence of buoyancy forces. Das et al. [59] examined entropy production in pseudo-plastic fluid flow in the existence of nanoparticles in a channel having permeable walls under convective heating. Analysis of heat transport in natural convection and entropy production inside a channel including a permeable plate mounted at the lower wall was performed numerically by Maskaniyan et al. [60]. Yusuf et al. [61] examined the entropy production number in the bioconvective flow of pseudoplastic fluid in the existence of nanoparticles along an aligned semi-infinite porous plate under convective boundaries, considering magnetic field, Joule heating, viscous dissipation, and chemical reaction. Olkha and Dadheech [62] numerically analysed entropy production in the flow of three different fluids (Williamson fluid, Casson fluid, and viscous fluid) produced by a permeable stretching sheet. Entropy production in the free convection of nanofluid via porous medium in a square configuration including heated corners, in the existence of Lorentz force, has been discussed by Reddy et al. [63]. Entropy production in Jeffery fluid flow in tilted permeable pipe via porous medium applying convective boundary constraints in the existence of an applied magnetic field has been investigated by Raje et al. [64]. In natural and forced convection slip flow in the region between vertical parallel permeable plates, entropy production has been discussed by Balamurugan et al. [65].

In view of the aforementioned studies, this work investigates gravity-driven Williamson fluid flow in the region bounded by two vertical parallel flat plates under convective surface boundary constraints. Slip flow is considered a porous medium under Lorentz force impact. In heat transport analysis, viscous dissipation, joule heating, and non-uniform heat source contributions are accounted for. Mass transport is also discussed in light of the existence of the reaction effect. Apart from that, second-law analysis is invoked in the study in terms of entropy production, which completes the heat transport analysis. The Runge-Kutta 4th order technique is employed for numerical simulations on MATLAB. Additionally, the influence of pertinent parameters on wall shear stress, rate of heat transport, and mass transport rate is exhibited in a graphical way and discussed. A comparison of the results obtained with previously published data shows an excellent match.

2. Problem formulation

We consider the fully developed, steady flow of an incompressible Williamson fluid in the region bounded by two vertical, infinitely parallel flat plates situated at a distance h apart (as **Figure 1** depicts). We choose $x-$axis parallel to the flow, opposite to the gravitational field, and $y-$ axis is considered perpendicular to it. The fluid flow is considered via porous medium, and a uniform magnetic field B_0 is applied in the perpendicular direction of flow. Convective boundary constraints relevant to heat and concentration are applied at the channel walls along with velocity

slip. Moreover, the impacts of viscous dissipation, exponential space-and thermal-dependent heat sources, joule heating, and higher-order chemical reactions are accounted for. A cartesian coordinate system is considered. The plates are assumed of infinite length in $x-$ and $z-$directions, all physical quantities are, therefore, treated as functions of y only.

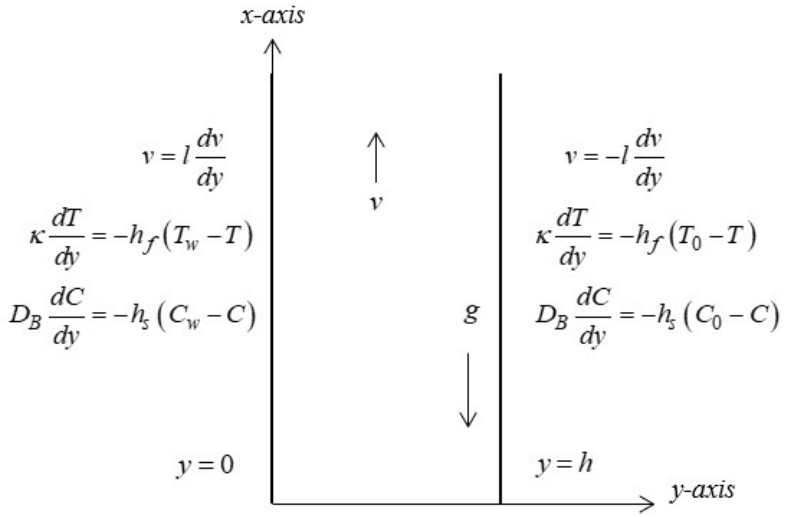

Figure 1. Systematic diagram for present problem.

With the aforementioned considerations, the regulating equations are

$$\mu\frac{d^2v}{dy^2} + \frac{\mu\Gamma}{\sqrt{2}}\frac{d}{dy}\left\{\left(\frac{dv}{dy}\right)^2\right\} + \rho g[\beta_T(T - T_0) + \beta_C(C - C_0)] - \frac{\mu}{K_p}v - \sigma B_0^2 v = 0 \tag{1}$$

$$\kappa\frac{d^2T}{dy^2} + \mu\left[1 + \frac{\Gamma}{\sqrt{2}}\frac{dv}{dy}\right]\left(\frac{dv}{dy}\right)^2 + Q_T^*(T - T_0) + Q_E^*(T_w - T_0) \times p\left(-\frac{y}{h}\right) + \sigma B_0^2 v^2 = 0 \tag{2}$$

$$D_B\frac{d^2C}{dy^2} - k_n(C - C_0)^n = 0 \tag{3}$$

and the relevant boundary constraints are considered as

$$\begin{aligned} &at\ y = 0: v = l\ \frac{dv}{dy}, \kappa\ \frac{dT}{dy} = -h_f(T_w - T), D_B\frac{dC}{dy} = -h_s(C_w - C), \\ &at\ y = h: v = -l\ \frac{dv}{dy}, \kappa\ \frac{dT}{dy} = -h_f(T_0 - T), D_B\frac{dC}{dy} = -h_s(C_0 - C), \end{aligned} \tag{4}$$

where v is the axial velocity of the fluid, T is the temperature of the fluid, T_0 is the temperature of the right wall, C is the concentration of the fluid, μ is the viscosity, ρ is the density, Γ is the time constant, β_T is the coefficient of thermal expansion, β_C is the coefficient of mass expansion, C_0 is the concentration at the right wall, σ is the electrical conductivity, B_0 is strength of magnetic field, K_p is the permeability of the porous medium, κ is the thermal conductivity, U is the reference velocity, h_f is the convective heat transfer coefficient, h_s is the convective mass transfer coefficient, D_B is diffusion coefficient, $Q_T{}^*$ is the thermal based heat source coefficient, $Q_E{}^*$ is the exponential heat source coefficient, T_w is temperature of left wall, C_w is the concentration at the left wall.

Invoking the following non-dimensional quantities

$$V = \frac{v}{U}, \eta = \frac{y}{h}, \theta = \frac{T - T_0}{T_w - T_0}, \phi = \frac{C - C_0}{C_w - C_0} \tag{5}$$

Equations (1)–(3) reduce to following non-dimensional form,

$$\frac{d^2V}{d\eta^2} + We\frac{dV}{d\eta}\frac{d^2V}{d\eta^2} + \frac{Gr}{Re}\theta + \frac{Gc}{Re}\phi - D\,V - Ha^2V = 0 \tag{6}$$

$$\frac{d^2\theta}{d\eta^2} + Br\left[1 + \frac{We}{2}\frac{dV}{d\eta}\right]\left(\frac{dV}{d\eta}\right)^2 + Q_T\theta + Q_E\,exp(-\eta) + Ha^2Br\,V^2 = 0 \tag{7}$$

$$\frac{d^2\phi}{d\eta^2} - ScK_n\phi^n = 0 \tag{8}$$

and the corresponding boundary conditions in non-dimensional form are:

$$\begin{aligned} V &= L\frac{dV}{d\eta}, \theta = 1 + \frac{1}{Bi_1}\frac{d\theta}{d\eta}, \phi = 1 + \frac{1}{Bi_2}\frac{d\phi}{d\eta}, at\ \eta = 0 \\ V &= -L\frac{dV}{d\eta}, \theta = \frac{1}{Bi_1}\frac{d\theta}{d\eta}, \phi = \frac{1}{Bi_2}\frac{d\phi}{d\eta}, at\ \eta = 1 \end{aligned} \tag{9}$$

where, $We = \sqrt{2}\,\Gamma U/h$ is the non-Newtonian parameter, $Br = \mu U^2/\kappa(T_w - T_0)$ is the Brinkman number, $Q_T = {Q_T}^* h^2/\kappa$ is the THS parameter, $Q_E = {Q_E}^* h^2/\kappa$ is the ESHS parameter, $Ha = B_0 h\sqrt{\sigma/\mu}$ is the Hartman number, $D = h^2/K_p$ is the porous medium parameter,$Gr = g\beta_T(T_w - T_0)h^3/\upsilon^2$ is the thermal Grashof number, $Gc = g\beta_C(C_w - C_0)h^3/\upsilon^2$ is the solutal Grashof number, $Re = Uh/\upsilon$ is Reynolds number, $Sc = \upsilon/D_B$ is the Schmidt number, $K_n = k_n(C_w - C_0)^{n-1}h^2/\upsilon$ is the chemical reaction parameter, $L = l/h$ is the velocity slip parameter, $Bi_1 = hh_f/\kappa$ is thermal Biot number, $Bi_2 = hh_s/D_B$ is the solutal Biot number.

3. Quantities of physical significance

The quantities of physical importance (skin-friction coefficient, Nusselt number, and Sherwood number) respectively, given by

$$C_f = \frac{\tau_w}{\mu\,U/h}, Nu = \frac{hq_w}{\kappa(T_w - T_0)}\ and\ Sh = \frac{hj_w}{D_B(C_w - C_0)} \tag{10}$$

where shear stress (τ_w), heat flux (q_w), and mass flux (j_w) are given by

$$\tau_w = \mu\left\{\frac{\partial v}{\partial y} + \frac{\Gamma}{\sqrt{2}}\left(\frac{\partial v}{\partial y}\right)^2\right\}_{y=0}, q_w = -\left(\kappa\frac{\partial T}{\partial y}\right)_{y=0}, j_w = -D_B\left(\frac{\partial C}{\partial y}\right)_{y=0} \tag{11}$$

On substituting values from Equation (11) and Equation (5) into Equation (10), the obtained non-dimensional expressions are as follows:

$$C_f = \left[\frac{dV}{d\eta} + \frac{We}{2}\left(\frac{dV}{d\eta}\right)^2\right]_{\eta=0}, Nu = -\left(\frac{d\theta}{d\eta}\right)_{\eta=0}, Sh = -\left(\frac{d\phi}{d\eta}\right)_{\eta=0} \tag{12}$$

4. Entropy generation

The dimensional entropy production for the current problem is given as

$$S_{gen} = \frac{\kappa}{{T_0}^2}\left(\frac{dT}{dy}\right)^2 + \left[\frac{RD}{C_0}\left(\frac{dC}{dy}\right)^2 + \frac{RD}{T_0}\left(\frac{dC}{dy}\frac{dT}{dy}\right)\right] + \frac{\mu}{T_0}\left[1 + \frac{\Gamma}{\sqrt{2}}\frac{du}{dy}\right] + \frac{1}{T_0}\frac{\mu}{k_p}u^2 + \frac{1}{T_0}\sigma{B_0}^2u^2 \tag{13}$$

where the terms on right side in Equation (13) are entropy contributions due to heat transport, mass transport, viscous dissipation, porous medium, and magnetic field respectively.

The non-dimensional entropy generation (NS) is defined as

$NS = \frac{S_{gen}}{S_0}$, where $S_0 = \frac{\kappa(T_w - T_0)^2}{{T_0}^2 h^2}$

Thus, the non-dimensional entropy production (NS) is expressed as

$$NS = \left(\frac{d\theta}{d\eta}\right)^2 + \frac{\Omega_C}{\Omega_T}\phi_C\left[\frac{\Omega_C}{\Omega_T}\left(\frac{d\phi}{d\eta}\right)^2 + \frac{d\theta}{d\eta}\frac{d\phi}{d\eta}\right] + \frac{Br}{\Omega_T}\left[\left(1 + \frac{We}{2}\frac{dV}{d\eta}\right)\left(\frac{dV}{d\eta}\right)^2 + (Ha)^2V^2 + DV^2\right] = S_T + S_C + S_f + S_M + S_P \quad (14)$$

where,

$S_T = \left(\frac{d\theta}{d\eta}\right)^2$, $S_C = \frac{\Omega_C}{\Omega_T}\phi_C\left[\frac{\Omega_C}{\Omega_T}\left(\frac{d\phi}{d\eta}\right)^2 + \frac{d\theta}{d\eta}\frac{d\phi}{d\eta}\right]$, $S_f = \frac{Br}{\Omega_T}\left(1 + \frac{We}{2}\frac{dV}{d\eta}\right)\left(\frac{dV}{d\eta}\right)^2$, $S_M = (Ha)^2V^2$, and $S_P = DV^2$ represent the irreversibility corresponding to heat transfer, mass transfer, viscous dissipation in porous medium, and magnetic field, respectively. $\Omega_T = (T_w - T_0)/T_0$ represent the temperature difference parameter, $\Omega_C = (C_w - C_0)/C_0$ represent the concentration difference parameter, $\phi_C = RDC_0/\kappa$ represent the diffusion parameter.

5. Numerical methodology

The Runge-Kutta fourth-order method with a shooting approach is utilized to tackle the system of nonlinear ODEs (6)-(8) numerically under the boundary conditions (9). Non-linear ODEs (6)-(8) including boundary constraints (9), are initially transformed into simultaneous nonlinear DEs of first order; they are then further changed into an initial value problem by applying the shooting approach.

$$\left(V, \frac{dV}{d\eta}, \theta, \frac{d\theta}{d\eta}, \phi, \frac{d\phi}{d\eta}\right) = (y_1, y_2, y_3, y_4, y_5, y_6) \quad (15)$$

$$\frac{dy_1}{d\eta} = y_2, \frac{dy_3}{d\eta} = y_4, \frac{dy_5}{d\eta} = y_6 \quad (16)$$

$$\frac{dy_2}{d\eta} = -\frac{\frac{Gr}{Re}y_3 + \frac{Gc}{Re}y_5 - Dy_1 - (Ha)^2 y_1}{1 + We\, y_2} \quad (17)$$

$$\frac{dy_4}{d\eta} = -Br\left(1 + \frac{We}{2}y_2\right){y_2}^2 - Q_T\, y_3 - Q_E\, exp(-\eta) - (Ha)^2 Br\, {y_1}^2 \quad (18)$$

$$\frac{dy_6}{d\eta} = ScK_n(y_5)^n \quad (19)$$

The boundary conditions are as follows:

$$y_1(0) = Ly_2(0), y_2(0) = \alpha_1, y_3(0) = 1 + \frac{1}{Bi_1}y_4(0), y_4(0) = \alpha_2, y_5(0) = 1 + \frac{1}{Bi_2}y_6(0), y_6(0) = \alpha_3, y_1(1) = -Ly_2(0), y_3(1) = \frac{1}{Bi_1}y_4(1), y_5(1) = \frac{1}{Bi_2}y_6(1) \quad (20)$$

where, α_1, α_2, and α_3 are the initial guesses.

6. Homotopy perturbation method

We use He's homotopy perturbation approach [66–68] to solve the presented problem analytically. According to HPM, the differential Equations (6)–(8) satisfied by $f(\eta)$, $\theta(\eta)$ and $\phi(\eta)$ are separated into two parts, the linear component $\mathscr{L}(f)$, $\mathscr{L}(\theta)$, and $\mathscr{L}(\phi)$ and the non-linear component $\mathcal{N}(f)$, $\mathcal{N}(\theta)$, and $\mathcal{N}(\phi)$ and may be expressed as follows:

$$\mathscr{L}(f) + \mathcal{N}(f) - g(\eta) = 0 \tag{21}$$

$$\mathscr{L}(\theta) + \mathcal{N}(\theta) - h(\eta) = 0 \tag{22}$$

$$\mathscr{L}(\phi) + \mathcal{N}(\phi) - I(\eta) = 0 \tag{23}$$

where $\mathscr{L}(V) = \frac{d^2V}{d\eta^2}$, $\mathscr{L}(\theta) = \frac{d^2\theta}{d\eta^2}$, $\mathscr{L}(\phi) = \frac{d^2\phi}{d\eta^2}$

$\mathcal{N}(V) = We\ \frac{dV}{d\eta}\frac{d^2V}{d\eta^2} + \frac{Gr}{Re}\theta + \frac{Gc}{Re}\phi - D\ V - Ha^2V,$

$\mathcal{N}(\theta) = Br\left[1 + \frac{We}{2}\frac{dV}{d\eta}\right]\left(\frac{dV}{d\eta}\right)^2 + Q_T\ \theta + Q_E\ exp(-\eta) + Ha^2Br\ V^2,$

$\mathcal{N}(\phi) = -ScK_n\phi^n$, $g(\eta) = 0$, $h(\eta) = 0$, and $I(\eta) = 0$. With the homotopy technique, we create a homotopy $\overline{V}(\eta, p)$: $\Omega \times [0,1] \to \mathbb{R}$, $\overline{\theta}(\eta, p)$: $\Omega \times [0,1] \to \mathbb{R}$, and $\overline{\phi}(\eta, p)$: $\Omega \times [0,1] \to \mathbb{R}$ which satisfies the following equation

$$(1-p)\left[\mathscr{L}\left(\overline{V}\right) - \mathscr{L}(u_0)\right] + p\left[\mathscr{L}\left(\overline{V}\right) + \mathcal{N}\left(\overline{V}\right) - g(\eta)\right] = 0, \qquad p \in [0,1] \tag{24}$$

$$(1-p)\left[\mathscr{L}\left(\overline{\theta}\right) - \mathscr{L}(\theta_0)\right] + p\left[\mathscr{L}\left(\overline{\theta}\right) + \mathcal{N}\left(\overline{\theta}\right) - h(\eta)\right] = 0, \qquad p \in [0,1] \tag{25}$$

$$(1-p)\left[\mathscr{L}\left(\overline{\phi}\right) - \mathscr{L}(\phi_0)\right] + p\left[\mathscr{L}\left(\overline{\phi}\right) + \mathcal{N}\left(\overline{\phi}\right) - I(\eta)\right] = 0, \qquad p \in [0,1] \tag{26}$$

Equations (24)–(26) can be written as

$$(1-p)\frac{d^2V}{d\eta^2} + p\left(\frac{d^2V}{d\eta^2} + We\ \frac{dV}{d\eta}\frac{d^2V}{d\eta^2} + \frac{Gr}{Re}\theta + \frac{Gc}{Re}\phi - D \times V - Ha^2V\right) = 0 \tag{27}$$

$$(1-p)\frac{d^2\theta}{d\eta^2} + p\left(\frac{d^2\theta}{d\eta^2} + Br\left[1 + \frac{We}{2}\frac{dV}{d\eta}\right]\left(\frac{dV}{d\eta}\right)^2 + Q_T\ \theta + Q_E\ exp(-\eta) + Ha^2Br \times V^2\right) = 0 \tag{28}$$

$$(1-p)\frac{d^2\phi}{d\eta^2} + p\left(\frac{d^2\phi}{d\eta^2} - ScK_n\phi^n\right) = 0 \tag{29}$$

In Equations (24)–(26), p is an embedding parameter, u_0, θ_0 and ϕ_0 is an initial guess, which satisfies the boundary conditions (9). It can be consider the solutions of the Equations (24)–(26) as a power series in p as follows:

$$\overline{V}(\eta, p) = \sum_{k=0}^{\infty} v_k(\eta)\, p^k \tag{30}$$

$$\overline{\theta}(\eta, p) = \sum_{k=0}^{\infty} \theta_k(\eta)\, p^k \tag{31}$$

$$\overline{\phi}(\eta, p) = \sum_{k=0}^{\infty} \phi_k(\eta)\, p^k \tag{32}$$

where v_k, θ_k, ϕ_k are unknown function of η. The approximate solutions (by taking $p \to 1$) are given by

$$V(\eta) = \overline{V}(\eta, 1) = \sum_{k=0}^{\infty} v_k(\eta) \tag{33}$$

$$\theta(\eta) = \overline{\theta}(\eta, 1) = \sum_{k=0}^{\infty} \theta_k(\eta) \tag{34}$$

$$\phi(\eta) = \overline{\phi}(\eta, 1) = \sum_{k=0}^{\infty} \phi_k(\eta) \tag{35}$$

using the Equations (9), (30)–(32) into Equations (24)–(26), equating the coefficients of like powers of p, we get

$$p^0: \frac{d^2v_0}{d\eta^2} = 0, v_0(0) = L\,\frac{dv_0(0)}{d\eta}, v_0(1) = -L\,\frac{dv_0(1)}{d\eta}$$
$$\frac{d^2\theta_0}{d\eta^2} = 0, \theta_0(0) = 1 + \frac{1}{Bi_1}\frac{d\theta_0(0)}{d\eta}, \theta_0(1) = \frac{1}{Bi_1}\frac{d\theta_0(1)}{d\eta} \quad (36)$$
$$\frac{d^2\phi_0}{d\eta^2} = 0, \phi_0(0) = 1 + \frac{1}{Bi_2}\frac{d\phi_0(0)}{d\eta}, \phi_0(1) = \frac{1}{Bi_2}\frac{d\phi_0(1)}{d\eta}$$

$$p^1: \frac{d^2v_1}{d\eta^2} + We\frac{dv_0}{d\eta}\frac{d^2v_0}{d\eta^2} + \frac{Gr}{Re}\theta_0 + \frac{Gc}{Re}\phi_0 - (D + Ha^2)v_0 = 0\,,$$
$$v_1(0) = L\frac{dv_1(0)}{d\eta}, v_1(1) = -L\frac{dv_1(1)}{d\eta}$$
$$\frac{d^2\theta_1}{d\eta^2} + Br\left(1 + \frac{We}{2}\frac{dv_0}{d\eta}\right)\left(\frac{dv_0}{d\eta}\right)^2 + Q_T\theta_0 + Q_Ee^{-\eta} + Ha^2Brv_0^2 = 0, \quad (37)$$
$$\theta_1(0) = \frac{1}{Bi_1}\frac{d\theta_1(0)}{d\eta}, \theta_1(1) = \frac{1}{Bi_1}\frac{d\theta_1(1)}{d\eta}$$
$$\frac{d^2\phi_1}{d\eta^2} - ScK_n\phi_0^n = 0, \phi_1(0) = \frac{1}{Bi_2}\frac{d\phi_1(0)}{d\eta}, \phi_1(1) = \frac{1}{Bi_2}\frac{d\phi_1(1)}{d\eta}$$

$$p^2: \frac{d^2v_2}{d\eta^2} + We\left(\frac{dv_0}{d\eta}\frac{d^2v_1}{d\eta^2} + \frac{dv_1}{d\eta}\frac{d^2v_0}{d\eta^2}\right) + \frac{Gr}{Re}\theta_1 + \frac{Gc}{Re}\phi_1 - (D + Ha^2)v_1 = 0\,,$$
$$v_2(0) = L\frac{dv_2(0)}{d\eta}, v_2(1) = -L\frac{dv_2(1)}{d\eta}$$
$$\frac{d^2\theta_2}{d\eta^2} + Br\left(2 + \frac{3}{2}We\frac{dv_0}{d\eta}\right)\frac{dv_0}{d\eta}\frac{dv_1}{d\eta} + Q_T\theta_1 + 2Ha^2Brv_0v_1 = 0, \quad (38)$$
$$\theta_2(0) = \frac{1}{Bi_1}\frac{d\theta_2(0)}{d\eta}, \theta_2(1) = \frac{1}{Bi_1}\frac{d\theta_2(1)}{d\eta}$$
$$\frac{d^2\phi_2}{d\eta^2} - nScK_n\phi_0^{n-1}\phi_1 = 0, \phi_2(0) = \frac{1}{Bi_2}\frac{d\phi_2(0)}{d\eta}, \phi_2(1) = \frac{1}{Bi_2}\frac{d\phi_2(1)}{d\eta}$$

Similarly, we can obtain other coefficients with the help of MATLAB software. Solving these linear ordinary differential equations using corresponding boundary conditions with the help of MATLAB and substituting in the Equations (33)–(35), we can find homotopy perturbation solutions for various values of parameters.

7. Results and discussion

In this section, various graphs are drawn to display the effects of various parameters that occurred in the problem. Throughout the numerical computations, we considered $Gr = 1$, $Ha = 0.3$, $D = 0.5$, $Br = 2$, $Q_T = 0.2$, $Q_E = 0.2$, $Re = 1$, $Sc = 0.5$, $K_n = 0.5$, $n = 2$, $L = 0.1$, $Gc = 1$, $Bi_1 = 100$, and $Bi_2 = 100$, as fixed. The MATLAB based RK-4th order technique is utilized to tackle the system of regulating Equations (6)–(8) along with boundary constraints (9). For the validity of the results obtained, a comparison is made with previously reported studies by Singh and Paul [69] and Ajibade et al. [23], as presented in **Table 1**. The validity of the study's findings is confirmed by a high level of agreement between the two sets of data.

Table 1. Comparison for $V(\eta)$ and $\theta(\eta)$ when $Re = Gr = 1.0$ and values of other parameters are taken zero.

η	Singh and Paul [69]		Ajibade et al. [23]		Present study			
					RK 4		HPM	
	$V(\eta)$	$\theta(\eta)$	$V(\eta)$	$\theta(\eta)$	$V(\eta)$	$\theta(\eta)$	$V(\eta)$	$\theta(\eta)$
0					0	1	0	1
0.1	0.02850	0.900	0.02819	0.900	0.02850	0.900	0.02850	0.900
0.2					0.04800	0.800	0.04800	0.800
0.3	0.05950	0.700	0.05916	0.700	0.05950	0.700	0.05950	0.700
0.4					0.06400	0.600	0.06400	0.600
0.5	0.06250	0.500	0.06238	0.500	0.06250	0.500	0.06250	0.500
0.6					0.05600	0.400	0.05600	0.400
0.7	0.04550	0.300	0.04553	0.300	0.04550	0.300	0.04550	0.300
0.8					0.03200	0.200	0.03200	0.200
0.9	0.01650	0.100	0.01653	0.100	0.01650	0.100	0.01650	0.100
1.0					0	0	0	0

Figures 2–10 show the impacts of various pertinent parameters such as thermal Grashof number (Gr), mass Grashof number (Gc), Reynolds number (Re), non-Newtonian fluid (Williamson fluid) parameter (We), Hartmann number (Ha), porous medium parameter (D), velocity slip parameter (L), chemical reaction parameter (K_n), thermal Biot number (Bi_1), solutal Biot number (Bi_2), Schmidt number (Sc), exponential space (Q_E) -and thermal-dependent (Q_T) heat source parameters, Brinkman number (Br), temperature difference parameter (Ω_T), concentration difference parameter (Ω_C), and diffusion parameter (ϕ_C) on fluid flow, thermal, and concentration fields.

The effects of D and Ha on the velocity distribution $V(\eta)$ are exhibited in **Figure 2**. It is observed, from this figure, $V(\eta)$ lessens with upsurge in the value parameter D. The reason behind this is that raising the porous medium parameter (or decreasing permeability) Darcy resistance which opposes the flow upsurges. Fluid flow also lowers with augmentation in Ha parameter value. An increase in Ha value results in increase of Lorentz force, which acts in a transverse direction. Hence, the flow field shrinks with the upsurging value of the parameter Ha.

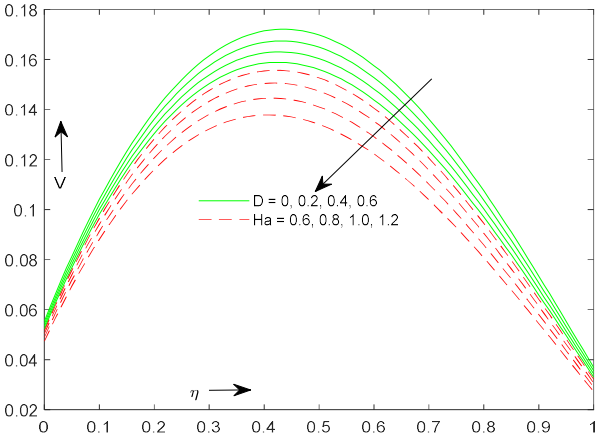

Figure 2. Velocity variation for D and Ha.

The impacts of Gr and Gc on fluid velocity $V(\eta)$ are displayed in **Figure 3**. We concluded, $V(\eta)$ enhances for increasing values of Gr and Gc because a greater Grashof number conveys a larger buoyancy force, which causes upsurge in velocity field.

Figure 4 illustrates the impact of Br and L on pace of the flow. With rising values of Br and L, fluid velocity $V(\eta)$ is found to grow. Upsurge in value of Br makes enhancement in viscous heating, which raises fluid kinetic energy and hence the pace of the flow improves. As the flow slip parameter (L) rises, the flow in the channel increases, and the effect is more apparent in the middle portion of the channel.

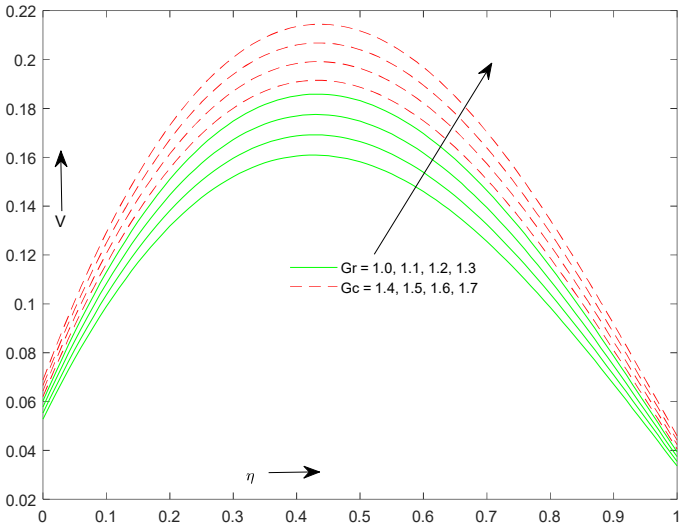

Figure 3. Velocity variation for Gr and Gc.

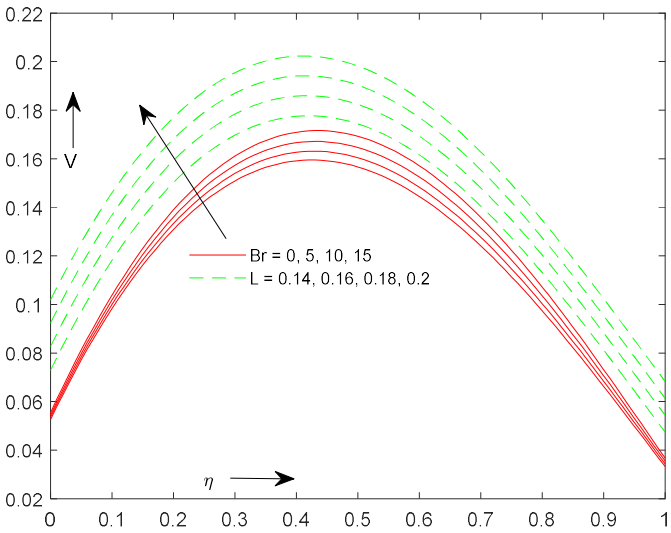

Figure 4. Velocity variation for L and Br.

Figure 5 depicts the impact of Re and We on velocity distribution. It is found that $V(\eta)$ lessens with rising value of Re. The impact of the Williamson parameter is also observed to shrink the velocity field. Physically, an upsurge in We parameter value implies an increase in stress relaxation time, which causes a reduction in fluid flow and thus lowers the velocity profile. The effect is prominent in almost half of the lower portion of the channel.

Figure 6 depicts the impacts of rising THS parameter and ESHS parameter values, i.e., Q_T and Q_E on the pace of the flow. The figure reveals that with a rise in the values of Q_T and Q_E fluid velocity increases. It may happen due to the higher kinetic energy of fluid molecules.

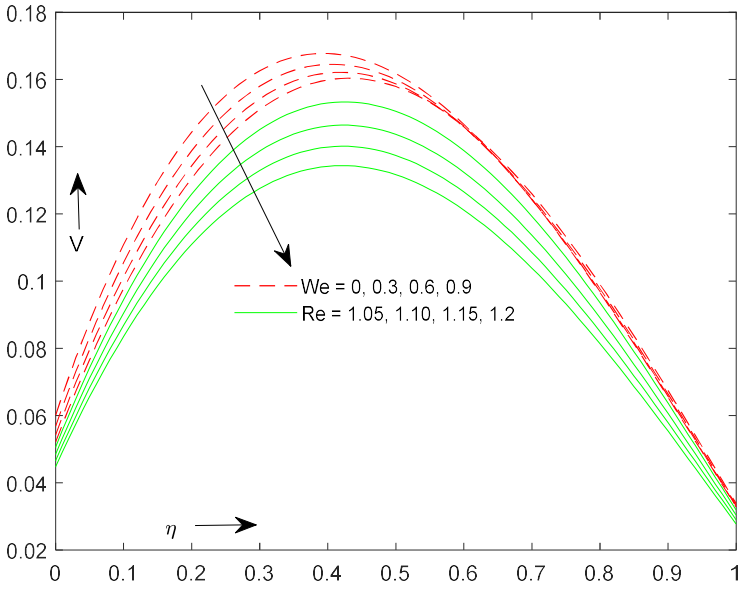

Figure 5. Velocity variation for We and Re.

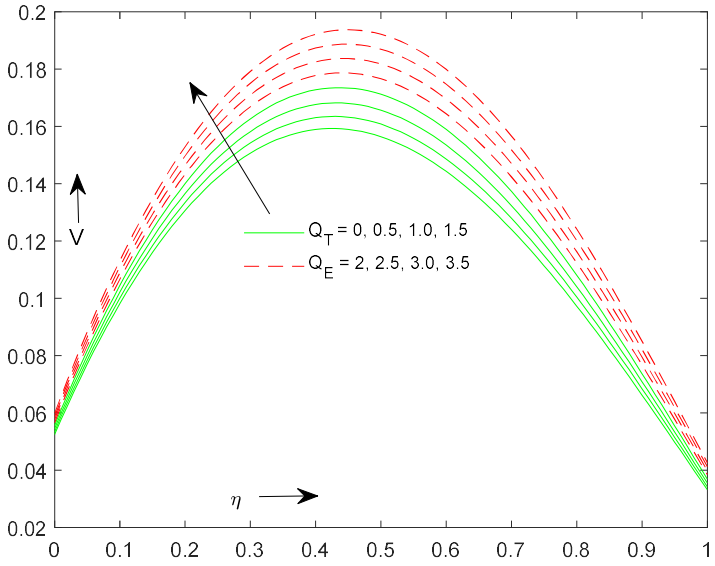

Figure 6. Velocity variation for Q_T and Q_E.

The effect of the THS and ESHS parameters i.e., (Q_T, and Q_E) on the energy profile $\theta(\eta)$ is exhibited in **Figure 7**. This graphical representation shows that when the value of Q_T and Q_E grows, the temperature profile improves because heat production improves as the values of heat source parameters (Q_T, and Q_E) increase.

Figure 8 reveals the effect of ascending Br and Bi_1 values on the temperature distribution $\theta(\eta)$. The figure displays that fluid temperature $\theta(\eta)$ increases with upsurging the values of Br and Bi_1. Physically, an increase in Brinkman number value enhances viscous heating, which causes an augmentation in fluid flow temperature and

thus the magnifies thermal profile. Thermal Biot number Bi_1 involves heat transfer coefficient. $Bi_1 = 0$, i.e., there is no heat transfer, and $Bi_1 > 0$ means heat transfer rate increases, which causes an increase in the temperature profile.

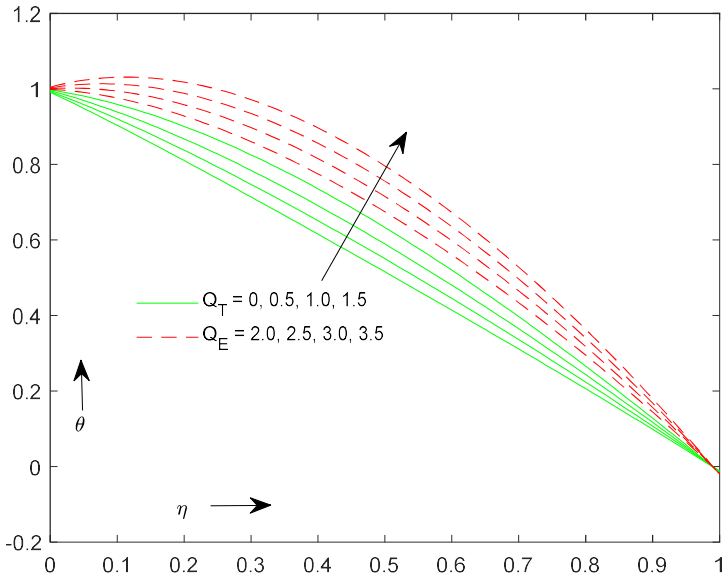

Figure 7. Temperature variation for Q_T and Q_E.

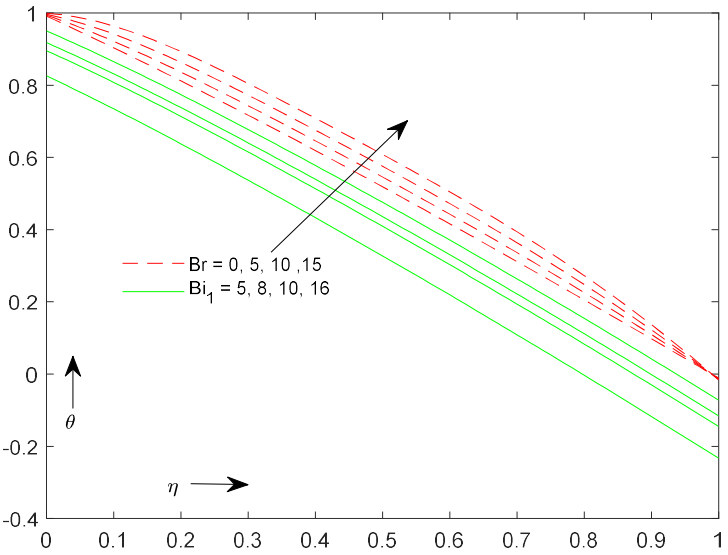

Figure 8. Temperature variation for Br and Bi_1.

Figure 9 indicates the variation in concentration distribution $\phi(\eta)$ corresponding to Sc and K_n. This figure depicts that concentration distribution, $\phi(\eta)$ is reducing with an augmentation in Sc and K_n values. The reason behind this is a reduction in mass diffusivity as the Schmidt number (Sc) value upsurges.

Figure 10 exhibits the variation in concentration distribution $\phi(\eta)$ for ascending values of n and Bi_2. It is quite obvious from these figures that $\phi(\eta)$ enhance for improving the values of n and Bi_2.

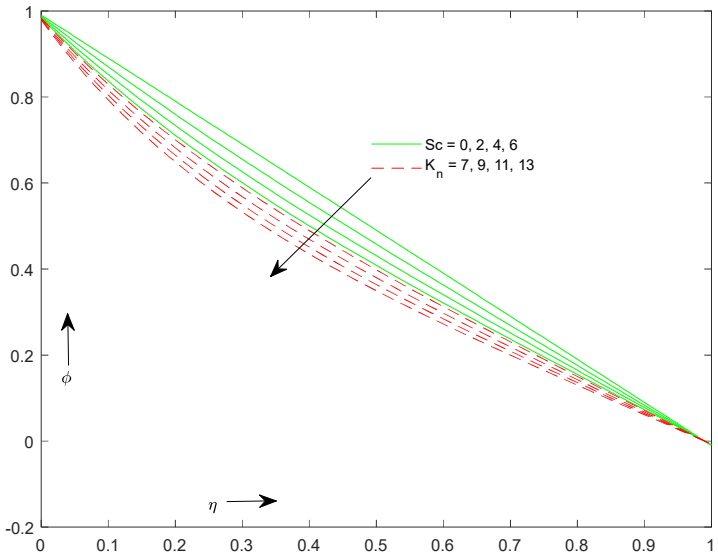

Figure 9. Concentration variation for Sc and K_n.

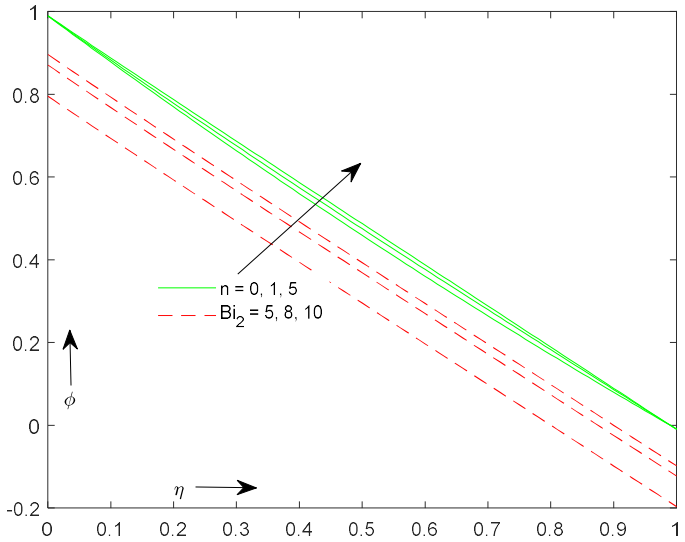

Figure 10. Concentration variation for n and Bi_2.

Figures 11–14 are sketched to depict the pertinent parameters impacting entropy production NS. These figures show more entropy production near the lower wall in comparison to that near the upper plate.

Figure 11 shows variation in NS due to the rising Brinkman number value. We observed, NS upsurges for ascending Br values. The reason behind, as Br is a parameter for viscous heating, and more heat is produced for larger values of Br which causes enhancement in NS and hence NS profile magnifies.

Figure 12 is drawn to exhibit the effect of Grashof numbers (Gr, and Gc) on NS. It depicts NS profile magnifies for ascending values of Grashof numbers, and the effect is significant in the entire channel width, and this is due to elevated friction (shear) near the walls.

Figure 13 is plotted to show the impact of Reynolds number (Re) and diffusion parameter (ϕ_C) on NS. It is noticed that an increase in Re values causes a reduction in NS and hence NS profile shrinks with ascending Reynolds number. This may be

attributed to the decrease in velocity, which results in a decrease in heat transfer and hence, a decrease in entropy generation. It is seen in this graph that upsurging value of the parameter ϕ_C cause upsurge in NS value and hence the corresponding profile improves. This is attributed to the increased convection currents driven by the differences in the densities of the fluid under the influence of gravitational forces, leading to increased heat production.

In **Figure 14,** the impact of the temperature difference parameter (Ω_T) and concentration difference parameter (Ω_C) is shown on the entropy generation number. The figure shows that the rising Ω_T value lowers NS and the corresponding profile diminishes due to the assumption that the temperature difference between the wall of the channel and fluid layers is sufficiently small. It depicts that irreversibility levels heightens with upsurge in Ω_C values. A greater mass is deposited on the surface of the plates as concentration increases, resulting in higher pressure being exerted on the walls of the plates, which causes higher rates of entropy generation.

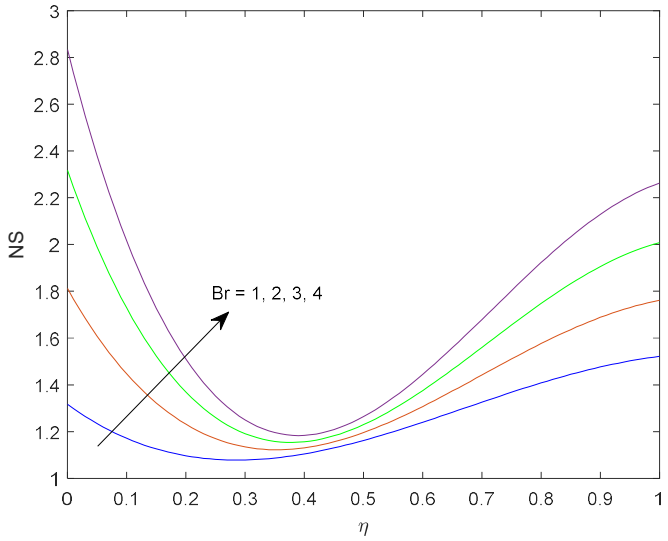

Figure 11. Entropy variation for Br.

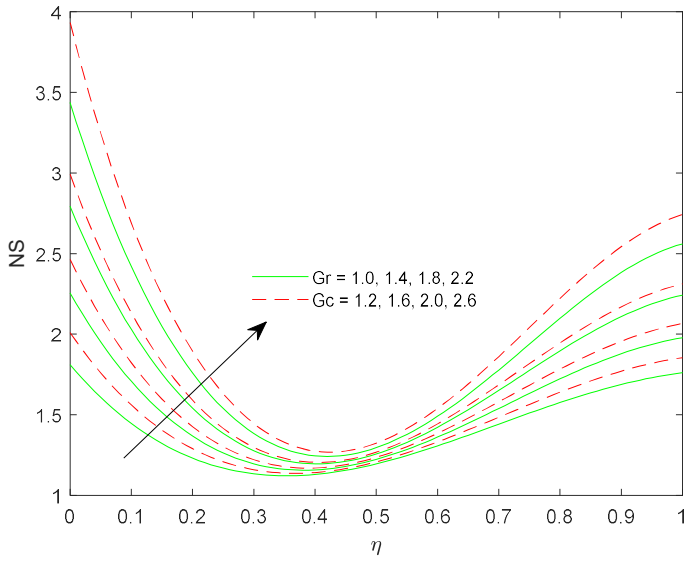

Figure 12. Entropy variation for Gr and Gc.

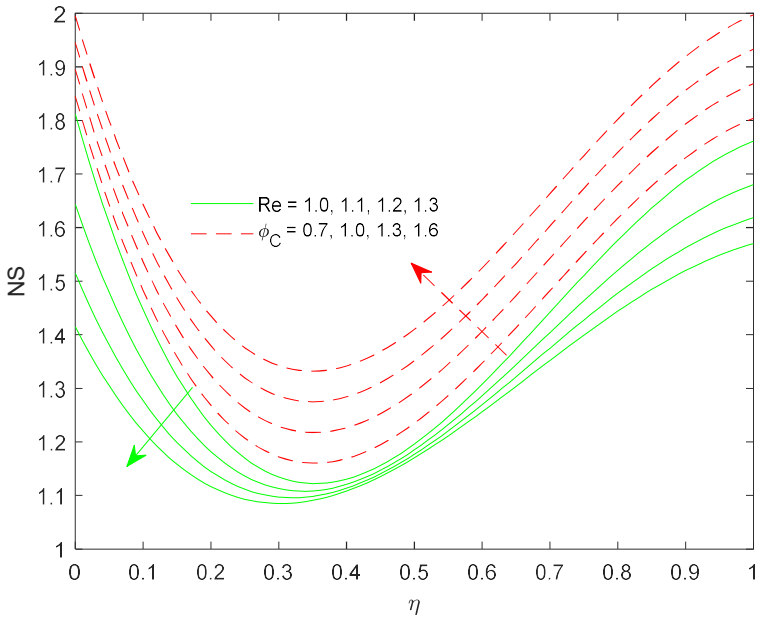

Figure 13. Entropy variation for Re and ϕ_C.

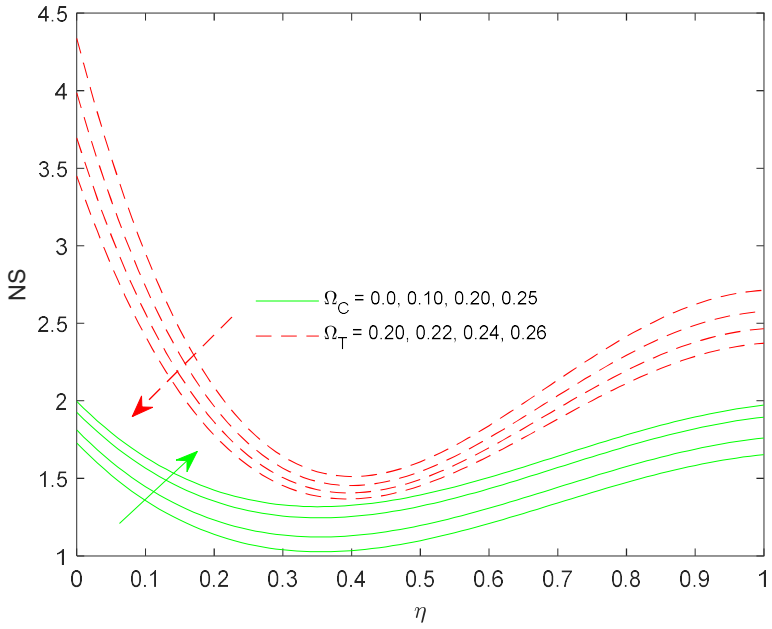

Figure 14. Entropy variation for Ω_T and Ω_C.

The values of the wall shear stress in terms of skin friction coefficient (C_f) and rate of heat transport in terms of Nusselt number (Nu) for the rising values of the relevant parameters are shown in **Figures 15** and **16**. It is observed that the wall shear stress decreases by raising the values of Re, Ha, D, while, the parameters: Gr and Gc enhance it. The Nusselt number decreases with the growing value of the parameters Br, Q_T, Q_E, and Bi_1 however, scenario changes in case of ascending values of Ha, as can be seen from the figure. Furthermore, **Figure 17** illustrates the variation in the Sherwood number (Sh) for ascending values of pertinent parameters. It is concluded that enhancement in values of the parameters K_n, Sc, Bi_2 augments Sh while, effect of the parameter n is seen to reduce it.

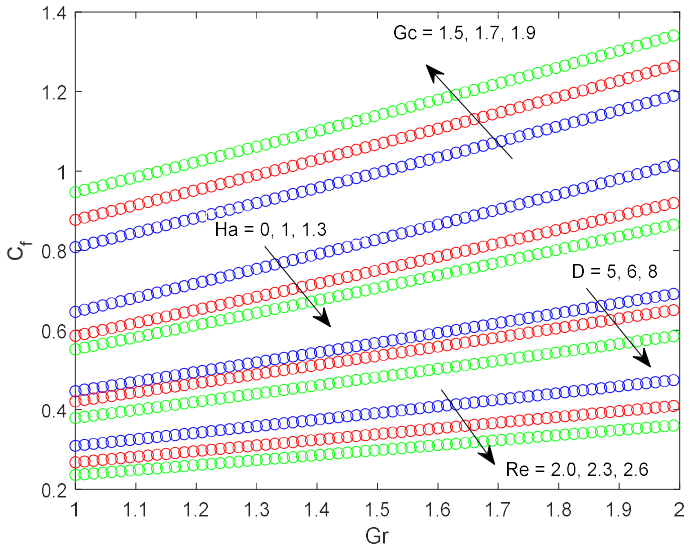

Figure 15. Skin friction coefficient for Gr, Gc, Ha, D, and Re.

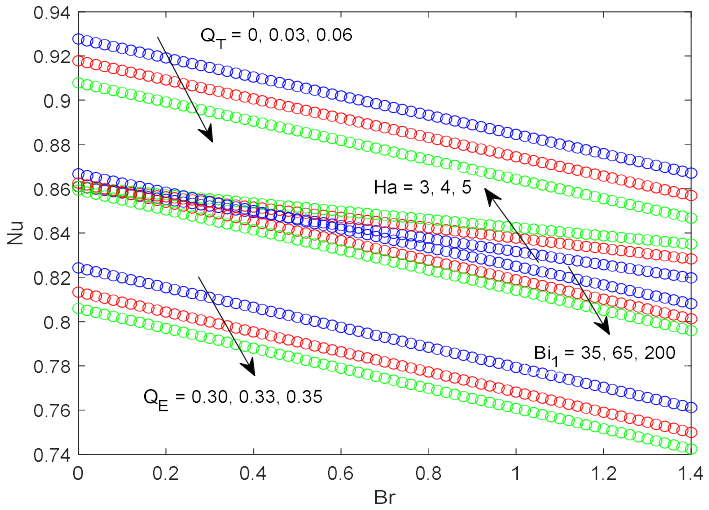

Figure 16. Nusselt number for Br, Q_T, Ha, Bi_1, and Q_E.

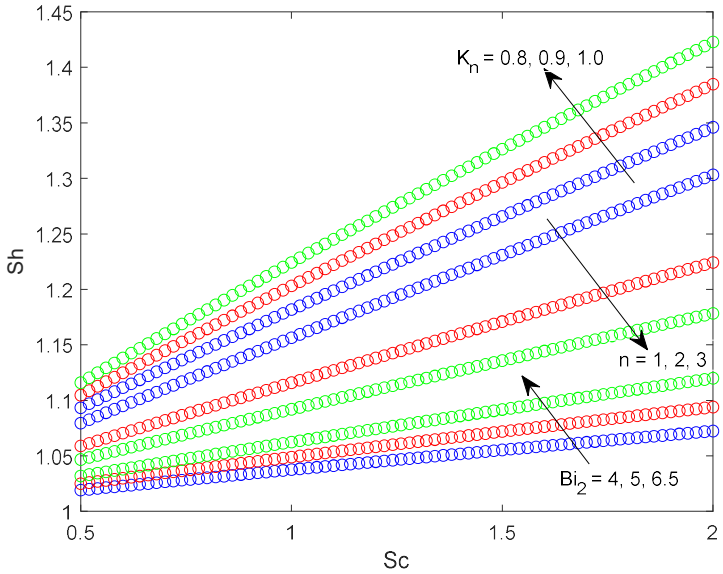

Figure 17. Sherwood number for Sc, K_n, n, and Bi_2.

8. Conclusions

In this research, we consider the fully developed steady-state laminar, natural convection flow of Williamson fluid in a vertical channel via porous medium. The velocity slip and the convective boundary conditions are applied. The contributions of higher order chemical reaction, viscous dissipation, Joule heating, and non-linear heat sources (ESHS/THS) are accounted for. Second-law analysis is presented in terms of entropy production. A numerical approach namely, Runge-Kutta 4th order is employed to tackle the problem with the shooting method. A comparison is also made using HPM (Homotopy Perturbation Method) in order to validate the findings. The conclusions of this study are:

1) Velocity field shrinks with rising values of D, Ha, Re, and We.
2) Velocity field upsurges with augmentation in values of Gr, Gc, Br, L, Q_T, and Q_E.
3) Temperature distribution magnifies with the rising values of Q_T, Q_E, Br, and Bi_1.
4) Concentration distribution increases for rising values of n and Bi_2, while it lessens for enhancement in values of Sc and K_n.
5) Entropy production upsurges as values of Br, Gr, Gc, Ω_T, and ϕ_C are increased, but it decreases as values of Re and Ω_T are increased.
6) Skin friction coefficient upsurges with enhancement in values of Gr and Gc while, the trend is changed in case of the parameters Re, Ha, D.
7) Nusselt number is observed to decrease with Br, Q_T, Q_E, and Bi_1 while, scenario changes in case of increasing values of Ha.
8) Rate of concentration transport upsurges with enhancement in values of K_n, Sc, and Bi_2 however, scenario changes in case of ascending values of n.

Author contributions: Conceptualization, AO and MK; methodology, MK; software, MK; validation, MK; formal analysis, AO and MK; investigation, MK; resources, MK; writing—original draft preparation, AO; writing—review and editing, AO and MK; visualization, MK; supervision, AO; project administration, AO. All authors have read and agreed to the published version of the manuscript.

Acknowledgments: The support provided by CSIR through the Senior Research Fellowship to Mukesh Kumar is gratefully acknowledged. The authors wish to express their thanks to the reviewers for their helpful comments and suggestions to improve the quality and presentation of this article.

Conflict of interest: The authors declare no conflict of interest.

References

1. Bruce RW, Na TY. Natural Convection Flow of Powell-Eyring Fluids between Two Vertical Flat Plates. ASME; 1967.
2. Aung W, Fletcher LS, Sernas V. Developing laminar free convection between vertical flat plates with asymmetric heating. International Journal of Heat and Mass Transfer. 1972, 15(11): 2293-2308. doi: 10.1016/0017-9310(72)90048-8
3. Vajravelu K, Sastri KS. Fully developed laminar free convection flow between two parallel vertical walls-I. International Journal of Heat and Mass Transfer. 1977, 20(6): 655-660. doi: 10.1016/0017-9310(77)90052-7
4. Rajagopal KR, Na TY. Natural convection flow of a non-Newtonian fluid between two vertical flat plates. Acta Mechanica. 1985, 54(3-4): 239-246. doi: 10.1007/bf01184849

5. Cheng CH, Kou HS, Huang WH. Flow reversal and heat transfer of fully developed mixed convection in vertical channels. Journal of Thermophysics and Heat Transfer. 1990, 4(3): 375-383. doi: 10.2514/3.190
6. Ziabakhsh Z, Domairry G. Analytic solution of natural convection flow of a non-Newtonian fluid between two vertical flat plates using homotopy analysis method. Communications in Nonlinear Science and Numerical Simulation. 2009, 14(5): 1868-1880. doi: 10.1016/j.cnsns.2008.09.022
7. Narahari M, Dutta BK. Free convection flow and heat transfer between two vertical parallel plates with variable temperature at one boundary. Acta Technica. 2011, 56: 103-113.
8. Kargar A, Akbarzade M. Analytic solution of natural convection flow of a non-newtonian fluid between two vertical flat plates using homotopy perturbation method (HPM). World Applied Sciences Journal. 2012, 20(11): 1459-1465. doi: 10.5829/idosi.wasj.2012.20.11.1707
9. Rashidi MM, Abelman S, Freidooni Mehr N. Entropy generation in steady MHD flow due to a rotating porous disk in a nanofluid. International Journal of Heat and Mass Transfer. 2013, 62: 515-525. doi: 10.1016/j.ijheatmasstransfer.2013.03.004
10. Hatami M, Hatami J, Jafaryar M, et al. Differential transformation method for Newtonian and Non-Newtonian fluids flow analysis: comparison with HPM and numerical solution. Journal of the Brazilian Society of Mechanical Sciences and Engineering. 2015, 38(2): 589-599. doi: 10.1007/s40430-014-0275-3
11. Raptis A, Massalas C, Tzivanidis G. Hydromagnetic free convection flow through a porous medium between two parallel plates. Physics Letters A. 1982, 90(6): 288-289. doi: 10.1016/0375-9601(82)90118-9
12. Chamkha AJ. Non-Darcy fully developed mixed convection in a porous medium channel with heat generation/absorption and hydromagnetic effects. Numerical Heat Transfer, Part A Applications. 1997, 32(6): 653-675. doi: 10.1080/10407789708913911
13. Singh KD, Pathak R. Effect of rotation and Hall current on mixed convection MHD flow through a porous medium filled in a vertical channel in presence of thermal radiation. Indian Journal of Pure & Applied Physics. 2012, 50: 77-85.
14. Das S, Jana RN, Makinde OD. An oscillatory MHD convective flow in a vertical channel filled with porous medium with Hall and thermal radiation effects. Special Topics & Reviews in Porous Media: An International Journal. 2014, 5(1): 63-82. doi: 10.1615/SpecialTopicsRevPorousMedia.v5.i1.60
15. Asha SK, Sunitha G. Effect of joule heating and MHD on peristaltic blood flow of Eyring–Powell nanofluid in a non-uniform channel. Journal of Taibah University for Science. 2019, 13(1): 155-168. doi: 10.1080/16583655.2018.1549530
16. Swain, BK, Parida BC, Kar S, et al. Viscous dissipation and joule heating effect on MHD flow and heat transfer past a stretching sheet embedded in a porous medium. Heliyon. 2020, 6(10): e05338. doi: 10.1016/j.heliyon.2020.e05338
17. Ramesh K, Riaz A, Dar ZA. Simultaneous effects of MHD and Joule heating on the fundamental flows of a Casson liquid with slip boundaries. Propulsion and Power Research. 2021, 10(2): 118-129. doi: 10.1016/j.jppr.2021.05.002
18. Ali A, Ahammad NA, Tag-Eldin E, et al. MHD williamson nanofluid flow in the rheology of thermal radiation, joule heating, and chemical reaction using the Levenberg–Marquardt neural network algorithm. Frontiers in Energy Research. 2022, 10. doi: 10.3389/fenrg.2022.965603
19. Williamson RV. The Flow of Pseudoplastic Materials. Industrial & Engineering Chemistry. 1929, 21(11): 1108-1111. doi: 10.1021/ie50239a035
20. Vasudev, R. Peristaltic Pumping of Williamson fluid through a porous medium in a horizontal channel with heat transfer. American Journal of Scientific and Industrial Research. 2010, 1(3): 656-666. doi: 10.5251/ajsir.2010.1.3.656.666
21. Subramanyam S, Reddy MVS, Reddy BJ. Influence of Magnetic Field on Fully Developed Free Convective Flow of a Williamson Fluid through a Porous Medium in a Vertical Channel. JAMFM. 2013, 5(1): 33-44.
22. Swaroopa B, Prasad KR. Influence of Radiation on MHD free Convective flow of a Williamson Fluid in a Vertical Channel. International Journal of Engineering and Technical Research. 2016, 5(2): 73-77.
23. Ajibade OA, Jha BK, Jibril HM, et al. Effects of dynamic viscosity and nonlinear thermal radiation on free convective flow through a vertical porous channel. International Journal of Thermofluids. 2021, 9: 100062. doi: 10.1016/j.ijft.2020.100062
24. Qawasmeh BR, Duwairi HM, Alrbai M. Non-Darcian forced convection heat transfer of Williamson fluid in porous media. Journal of Porous Media. 2021, 24(8): 23-35. doi: 10.1615/JPorMedia.2021025540
25. Pattanaik PC, Mishra SR, Jena S, et al. Impact of radiative and dissipative heat on the Williamson nanofluid flow within a parallel channel due to thermal buoyancy. Proceedings of the Institution of Mechanical Engineers. 2022, 236(1-2): 3-18. doi: 10.1177/23977914221080046

26. Usman, Shaheen S, Arain MB, et al. A case study of heat transmission in a Williamson fluid flow through a ciliated porous channel: A semi-numerical approach. Case Studies in Thermal Engineering. 2023, 41: 102523. doi: 10.1016/j.csite.2022.102523
27. Grosan T, Pop R, Pop I. Thermophoretic deposition of particles in fully developed mixed convection flow in a parallel-plate vertical channel. Heat and Mass Transfer. 2009, 45(4): 503-509. doi: 10.1007/s00231-008-0443-z
28. Ibrahim FS, Hady FM, Abdel-Gaied SM, et al. Influence of chemical reaction on heat and mass transfer of non-Newtonian fluid with yield stress by free convection from vertical surface in porous medium considering Soret effect. Applied Mathematics and Mechanics. 2010, 31: 675-684. doi: 10.1007/s10483-010-1302-9
29. Uwanta IJ, Hamza MM. Effect of suction/injection on unsteady hydromagnetic convective flow of reactive viscous fluid between vertical porous plates with thermal diffusion. International Scholarly Research Notices. 2014, 2014. doi: 10.1155/2014/980270
30. Prasannakumara BC, Gireesha BJ, Gorla R, et al. Effects of chemical reaction and nonlinear thermal radiation on Williamson nanofluid slip flow over a stretching sheet embedded in a porous medium. Journal of Aerospace Engineering. 2015, 29(5): 04016019. doi: 10.1061/(ASCE)AS.1943-5525.0000578
31. Singh K, Kumar M. Influence of chemical reaction on heat and mass transfer flow of a micropolar fluid over a permeable channel with radiation and heat generation. Journal of Thermodynamics. 2016, 2016: 8307980. doi: 10.1155/2016/8307980
32. Mallikarjun P, Murthy RV, Mahabaleshwar US, et al. Finite-Element Analysis of Fully Developed Mixed Convection through a Vertical Channel in the Presence of Heat Generation/Absorption with a First-Order Chemical Reaction. Defect and Diffusion Forum. 2018, 388: 394-406. doi: 10.4028/www.scientific.net/DDF.388.394
33. Loganathan P, Dhivya M. Heat and mass transfer analysis of a convective Williamson fluid flow over a cylinder. International Journal of Fluid Mechanics Research. 2020, 47(2): 171-189. doi: 10.1615/InterJFluidMechRes.2020027371
34. Huang JS. Chemical reaction and activation energy on heat and mass transfer for convective flow along an inclined surface in Darcy porous medium with Soret and Dufour effects. Journal of Mechanics. 2023, 39: 88-104. doi: 10.1093/jom/ufad006
35. Nazir S, Kashif M, Zeeshan A, et al. A study of heat and mass transfer of non-Newtonian fluid with surface chemical reaction. Journal of the Indian Chemical Society. 2022, 99(5): 100434. doi: 10.1016/j.jics.2022.100434
36. Olkha A, Kumar M. Casson fluid flow in a vertical annulus through porous medium with heat transfer characteristics and chemical reaction: An exact solution. IJMPC. 2022, 34(6): 2350078. doi: 10.1142/S012918312350078X
37. Olkha A, Kumar M. Heat transfer characteristics in non-Newtonian fluid flow due to a naturally permeable curved surface and chemical reaction. Heat Transfer. 2023, 52: 5431–5453. doi: 10.1002/htj.22934
38. Srinivas S, Malathy T, Reddy AS. A note on thermal-diffusion and chemical reaction effects on MHD pulsating flow in a porous channel with slip and convective boundary conditions. JKSUES. 2016, 28(2): 213-221. doi: 10.1016/j.jksues.2014.03.011
39. Oyelakin IS, Mondal S, Sibanda P. Unsteady Casson nanofluid flow over a stretching sheet with thermal radiation, convective and slip boundary conditions. Alexandria Engineering Journal. 2016, 55(2): 1025-1035. doi: 10.1016/j.aej.2016.03.003
40. Sharada K, Shankar B. Effect of partial slip and convective boundary condition on MHD mixed convection flow of Williamson fluid over an exponentially stretching sheet in the presence of joule heating. Global Journal of Pure and Applied Mathematics. 2017, 13(9): 5965-5975.
41. Zeeshan A, Shehzad N, Ellahi R. Analysis of activation energy in Couette-Poiseuille flow of nanofluid in the presence of chemical reaction and convective boundary conditions. Results in Physics. 2018, 8: 502-512. doi: 10.1016/j.rinp.2017.12.024
42. Neeraja A, Devi RR, Devika B, et al. Effects of viscous dissipation and convective boundary conditions on magnetohydrodynamics flow of casson liquid over a deformable porous channel. RINENG. 2019, 4: 100040. doi: 10.1016/j.rineng.2019.100040.
43. Jagadeesh S, Reddy MCK. Convection of 3D MHD non-Newtonian couple stress nanofluid flow via stretching surface. Heat Transfer. 2022, 52(2): 1081-1096. doi: 10.1002/htj.22730
44. Zia QZ, Ullah I, Waqas MA, et al. Cross diffusion and exponential space dependent heat source impacts in radiated three-dimensional (3D) flow of Casson fluid by heated surface. Results in Physics. 2018, 8: 1275-1282. doi: 10.1016/j.rinp.2018.01.001
45. Thriveni K, Mahanthesh B, Giulio L et al. Significance of induced magnetic field and exponential space dependent heat source on quadratic convective flow of Casson fluid in a micro-channel via HPM. Mathematical Modelling of Engineering

Problems. 2019, 6(3): 369-384. doi: 10.18280/mmep.060308
46. Mahanthesh B, Lorenzini G, Oudina FM, et al. Significance of exponential space-and thermal-dependent heat source effects on nanofluid flow due to radially elongated disk with Coriolis and Lorentz forces. Journal of Thermal Analysis and Calorimetry. 2020, 141: 37-44. doi: 10.1007/s10973-019-08985-0
47. Nagaraja B, Gireesha BJ. Exponential space-dependent heat generation impact on MHD convective flow of Casson fluid over a curved stretching sheet with chemical reaction. Journal of Thermal Analysis and Calorimetry. 2021, 143(6): 4071-4079. doi: 10.1007/s10973-020-09360-0
48. Swain K, Animasaun IL, Ibrahim SM. Influence of exponential space-based heat source and Joule heating on nanofluid flow over an elongating/shrinking sheet with an inclined magnetic field. International Journal of Ambient Energy. 2021, 43(1): 1-13. doi: 10.1080/01430750.2021.1873854
49. Hasibi A, Gholami A, Asadi Z et al. Importance of Induced Magnetic Field and Exponential Heat Source on Convective Flow of Casson Fluid in a Micro-channel via AGM. Theoretical and Applied Mechanics Letters. 2022, 12(3): 100342. doi: 10.1016/j.taml.2022.100342
50. Sharma BK, Kumar A, Gandhi R, et al. Exponential space and thermal-dependent heat source effects on electro-magneto-hydrodynamic Jeffery fluid flow over a vertical stretching surface. International Journal of Modern Physics B. 2022, 36(30): 2250220. doi: 10.1142/S0217979222502204
51. Yessef M, Bossoufi B, Taoussi M, et al. Improving the maximum power extraction from wind turbines using a second-generation CRONE controller. Energies. 2022, 15(10): 3644. doi: 10.3390/en15103644
52. Chojaa H, Derouich A, Zamzoum O, et al. Robust control of DFIG-based WECS integrating an energy storage system with intelligent MPPT under a real wind profile. IEEE Access. 2023, 11: 90065-90083. doi: 10.1109/ACCESS.2023.3306722
53. Loulijat A, Chojaa H, El marghichi M, et al. Enhancement of LVRT Ability of DFIG Wind Turbine by an Improved Protection Scheme with a Modified Advanced Nonlinear Control Loop. Processes. 2023, 11(5): 1417. doi: 10.3390/pr11051417
54. Hamid C, Aziz D, Zamzoum O, et al. Robust Control System for DFIG-Based WECS and Energy Storage in reel Wind Conditions. EAI Endorsed Transactions on Energy Web. 2024, 11. doi: 10.4108/ew.4856
55. Bejan A. A study of entropy generation in fundamental convective heat transfer. ASME Journal of Heat and Mass Transfer. 1979, 101(4): 718-725. doi: 10.1115/1.3451063
56. Bejan A. Short Communication Notes on the History of the Method of Entropy Generation Minimization (Finite Time Thermodynamics). Journal of Non-Equilibrium Thermodynamics. 1996, 21(3): 239-242. doi: 10.1515/jnet.1996.21.3.239
57. Baytas AC. Entropy generation for natural convection in an inclined porous cavity. International Journal of Heat and Mass Transfer. 2000, 43(12): 2089-2099. doi: 10.1016/S0017-9310(99)00291-4
58. Makinde OD, Eegunjobi AC. Entropy generation in a couple stress fluid flow through a vertical channel filled with saturated porous media. Entropy. 2013, 15(11): 4589-4606. doi: 10.3390/e15114589
59. Das S, Banu AS, Jana RN, et al. Entropy analysis on MHD pseudo-plastic nanofluid flow through a vertical porous channel with convective heating. Alexandria Engineering Journal. 2015, 54(3): 325-337. doi: 10.1016/j.aej.2015.05.003
60. Maskaniyan M, Nazari M, Rashidi S, et al. Natural convection and entropy generation analysis inside a channel with a porous plate mounted as a cooling system. TSEP. 2018, 6: 186-193. doi: 10.1016/j.tsep.2018.04.003
61. Yusuf TA, Mabood F, Prasannakumara BC et al. Magneto-bioconvection flow of Williamson nanofluid over an inclined plate with gyrotactic microorganisms and entropy generation. Fluids. 2021, 6(3): 109. doi: 10.3390/fluids6030109
62. Olkha A, Dadheech A. Second Law Analysis for Radiative Magnetohydrodynamics Slip Flow for Two Different Non-Newtonian Fluid with Heat Source. Journal of Nanofluids. 2021, 10(3): 447-461. doi: 10.3390/fluids6030109
63. Reddy PBA, Salah T, Jakeer S, et al. Entropy generation due to magneto-natural convection in a square enclosure with heated corners saturated porous medium using Cu/water nanofluid. Chinese Journal of Physics. 2022, 77: 1863-1884. doi: 10.1016/j.cjph.2022.01.012
64. Raje A, Bhise AA, Kulkarni A. Entropy analysis of the MHD Jeffrey fluid flow in an inclined porous pipe with convective boundaries. International Journal of Thermofluids. 2023, 17: 100275. doi: 10.1016/j.ijft.2022.100275
65. Balamurugan KS, Varma NU, Prasad JLR. Entropy generation analysis on forced and free convection flow in a vertical porous channel with aligned magnetic field and Navier slip. Heat Transfer. 2023. doi: 10.1002/htj.22897
66. He JH. Homotopy perturbation technique. Computer Methods in Applied Mechanics and Engineering. 1999, 178(3-4): 257-262. doi: 10.1016/S0045-7825(99)00018-3

67. He JH. Homotopy perturbation method: a new nonlinear analytical technique. Applied Mathematics and Computation. 2003, 135(1): 73-79. doi: 10.1016/S0096-3003(01)00312-5
68. He JH. An elementary introduction to recently developed asymptotic methods and nanomechanics in textile engineering. International Journal of Modern Physics B. 2008, 22(21): 3487-3578. doi: 10.1142/s0217979208048668
69. Singh AK and Paul T. Transient natural convection between two vertical walls heated/cooled asymmetrically. International Journal of Applied Mechanics and Engineering. 2006, 11(1): 143-154.